Total scattering cross section of spin-polarized low-energy electrons in transition metals

Henri-Jean Drouhin
Laboratoire de Physique de la Matière Condensée (UMR 7643-CNRS), Ecole Polytechnique, 91128 Palaiseau cedex, France
(Received 13 December 1999)

We analyze the low-energy (5–50 eV) electron inelastic mean free path in transition metals in the framework of a simple density-of-state model. We establish relations between the scattering cross section and the hole numbers. This allows us to disentangle the different electron-electron scattering channels and, using recently available experimental data, to probe the energy dependence of the exchange matrix element. A critical review of the literature leads us to propose numerical mean free path expressions, relevant for several materials.

I. INTRODUCTION

Information on the inelastic electron mean free path (IMFP) in metals is essential for electron spectroscopies. Theoretical and experimental investigations started many years ago[1,2] and the study of magnetic properties became especially active with the development of efficient spin-polarized electron sources.[3] Theoretical models using refined formalism were proposed, leading us to predict different spin-dependent effects.[4,5] It must be stressed that direct accurate measurements are intrinsically difficult. In its principle, an IMFP determination is straightforward, as it is obtained by measuring the attenuation versus thickness of an electron beam traveling at a given energy. But practically, this implies the need to extract an extremely small signal originating from true ballistic electrons from a large background. Different stray effects crucially depend on the sample under investigation. In particular, because the IMFP is expected to decrease when increasing primary energy (up to about 100 eV), the ballistic contribution should be exponentially vanishing and is easily polluted by a minute number of electrons propagating through uncontrolled channels, pin holes or defects in the material, for instance. Moreover, as the transmitted current also exponentially decreases with increasing metal thickness, only a narrow thickness range can be investigated, which is generally further restricted by constraints due to the growth process: a minimum metal thickness can be required to obtain a continuous layer, the structural properties depend on the substrate and on the growth conditions and, in the case of ferromagnetic metals, the magnetic properties may differ at low coverage.[6] The electron IMFP can alternatively be deduced from the fit of the energy distribution of the photoemitted electrons, which is, however, a less direct method,[7–10] or from the study of the photoemission yield (possibly including spin-polarization measurements) from a substrate covered by an overlayer of growing thickness.[11,12] In magnetic materials, the spin-dependent part of the IMFP can be more easily determined with accuracy as any parasitic effects are eliminated by reversing either the target magnetization or the primary beam polarization, which is a decisive advantage. This point of view was taken by Oberli *et al.*,[13] who tried to relate the IMFP to its spin-dependent part, or, in other words, the total scattering cross section to its spin-dependent component. In the following, we derive expressions for the spin-dependent electron mean free path, on the basis of simple physical assumptions, and we thoroughly test them by comparison with a number of experimental data.

II. THEORETICAL IMFP VARIATION

A. A (too) simple model

It is reasonable to think that, in transition metals, the IMFP variation is mostly determined by density-of-state effects, whereas the transition matrix elements introduce weaker corrections. The crudest model was given by Schönhense and Siegmann,[14] who *phenomenologically* relate the ''scattering cross section'' σ^+ (σ^-) for majority-spin (minority-spin) electrons to the numbers of holes per atom in the *d* bands. This model was an important contribution to the understanding of spin-dependent effects in the experiments involving low-energy electrons. First, let us remind that, generally speaking, an electron scattering cross section σ_e is connected to the electron mean free path λ_e by the relation $\lambda_e \sigma_e N = 1$, where N is the density of scattering centers. In Ref. 14, to make more evident that the *d* holes act as scattering centers, the scattering cross section is somewhat improperly defined as the inverse of the IMFP. Here, we will keep this terminology as we start from the well-known (see, for instance, Ref. 5) Schönhense and Siegmann model to define notations making more easy the comparison between different papers in the literature. These authors write

$$\sigma^{\pm} = \sigma_0 + \sigma_d (5 - n^{\pm}) = \sigma_0 + \sigma_d N_h^{\pm}, \tag{1}$$

where σ_0 and σ_d, respectively, refer to *sp* and *d* contributions and are *assumed to be material independent*. This is somewhat surprising, as, for instance, the atomic concentration—and thus the concentration of the electron gas—in the metals under consideration are rather different.[15] n^+ (n^-) is the number of up- (down-) spin electrons in the *d* bands. For the following discussion, we have introduced the hole numbers in the majority- and minority-spin *d* bands, $N_h^{\pm} = 5 - n^{\pm}$, the total hole number $\mathcal{N}_h = N_h^- + N_h^+$ and the difference $\Delta\mathcal{N}_h = N_h^- - N_h^+ = n^+ - n^-$. It should be remarked that the spin-averaged cross section is

$$\langle\sigma\rangle=\frac{\sigma^-+\sigma^+}{2}=\sigma_0+\sigma_d\frac{\mathcal{N}_h}{2}. \tag{2}$$

Writing $n^{\pm}=n\pm\Delta n$, the number of Bohr magnetons is expressed as $n_B=n^+-n^-=2\Delta n$ and

$$\Delta\sigma=\sigma^--\sigma^+=\sigma_d n_B=\sigma_d\Delta\mathcal{N}_h. \tag{3}$$

The Schönhense and Siegmann formula [Eq. (1)] originates from the naive picture of a primary electron ''falling'' into empty states in the *d* bands, with spin conservation. In a natural way, σ_d is interpreted as the scattering cross section for scattering by the holes in the *d* bands. As $\sigma^{\pm}$ is proportional to $(\lambda^{\pm})^{-1}$, the inverse of the mean free path for majority- and minority-spin electrons, the IMFP asymmetry *A* is

$$\begin{aligned}A&=\frac{\sigma^--\sigma^+}{\sigma^-+\sigma^+}\\&=\frac{\lambda^+-\lambda^-}{\lambda^++\lambda^-}\\&=\frac{\Delta n}{(\sigma_0/\sigma_d)+5-n}=\frac{1}{2}\,\frac{\Delta\mathcal{N}_h}{(\sigma_0/\sigma_d)+\dfrac{\mathcal{N}_h}{2}}.\end{aligned} \tag{4}$$

The spin-dependent component $\Delta\sigma$ and the IMFP asymmetry *A* play a central role in spin-polarized electron experiments and can be determined by different methods (see the Appendix).

From a compilation of experimental spin-averaged IMFP measurements in several metals, plotted versus $\mathcal{N}_h/2$, it is deduced in Ref. 16 that $\sigma_0/\sigma_d\sim 0.7\cdots$ but it is also found that this value is inconsistent with the *A* determination from the cascade polarization measurement. To fit the *A* experimental data, the ratio σ_0/σ_d has to be increased up to 2.5! In fact, this quantitative inconsistency between the two σ_0/σ_d determinations reveals a deep failure of the model. Looking more carefully at the implications of the postulated relation between $\sigma^{\pm}$ and the hole numbers makes it obvious that the starting point is unphysical: indeed, in the extreme case of a strong ferromagnet (with all-occupied majority-spin states), the majority-spin scattering cross section is independent of the total hole number and the mean free path deduced from attenuation measurements through thick layers will be almost the mean free path of the majority-spin electrons [when the layer is thick enough, see Sec. 1, Eq. (A10), of the Appendix], as it is much larger than the mean free path of the minority-spin electrons. On the contrary, we must keep in mind that majority-spin electrons propagating in the metal can always lose a small amount of energy and excite minority-spin electrons inside the minority-spin band so that *any correct expression for the majority-spin cross section should contain the number of holes in the minority-spin band*. An important consequence is also, as we will see, that the relation $\Delta\sigma=n_B\sigma_d$, which is the basis for the total scattering cross section determination proposed in Ref. 13, does not hold.

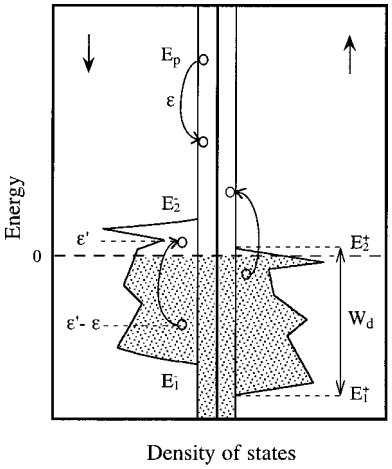

FIG. 1. Principle of the calculation. For each spin, the band structure is described by a constant density of states in the *sp* band on which is superimposed a positive continuous compact-support function describing the *d* band. The *d* bands are bounded by energies $E_1^{\pm}$ and $E_2^{\pm}$, their common width is denoted as W_d. The dotted area represents the occupied states, located below the Fermi level (energy origin). In the figure, a primary electron at energy E_p with a minority spin, loses an amount of energy ε, which is used to excite a secondary electron from a negative energy $\varepsilon'-\varepsilon$ to a positive energy ε', with spin conservation. This occurs either in the minority-spin band (direct processes) or in the majority-spin band (exchange like processes).

B. A simple physical model

We now use a density-of-states model proposed in Ref. 17, which only takes into account electron-electron scattering in the framework of the random-*k* approximation.[7,18] We consider a primary electron at energy E_p (hereafter the energy origin is set at the metal Fermi level) with a spin $\sigma=\pm$. This electron loses an amount of energy ε, which is used to excite a secondary electron from a negative energy $\varepsilon'-\varepsilon$ to a positive energy ε', with spin conservation. The band structure is described by a constant density of states n_{sp} for the *sp* band on which is superimposed a positive continuous compact-support function $n_d^{\sigma}(u)$ describing the considered *d* band: $n^{\sigma}(u)=n_d^{\sigma}(u)+n_{sp}$. The *d* bands are bounded by energies E_1^{σ} (lower bound) and E_2^{σ} (upper bound), their common width is denoted as W_d (see Fig. 1). The band centers E_d^{σ} and the centers of the emerged part of the *d* bands, E_h^{σ}, are defined as

$$5E_d^{\sigma}=\int_{-\infty}^{+\infty}un_d^{\sigma}(u)du;\quad N_h^{\sigma}E_h^{\sigma}=\int_0^{+\infty}un_d^{\sigma}(u)du. \tag{5}$$

This implies that the densities of states are normalized to individual atoms. Other relevant quantities are defined in the following way: $E_d=-(E_d^-+E_d^+)/2$, $\mathcal{N}_hE_h=(N_h^-E_h^-+N_h^+E_h^+)$, $\Delta\mathcal{N}_hE_h'=(N_h^-E_h^--N_h^+E_h^+)$, and $\gamma\mathcal{N}_h=[(N_h^-)^2+(N_h^+)^2]$. Assuming that all transitions have an equal weight ω, the low-energy scattering rates for $E_p\geqslant W+\sup(0,E_2^-,E_2^+)$, where $W=\sup(|E_1^+|,|E_2^+|,|E_1^-|,|E_2^-|,W_d)$ is shown to be

$$R^{\sigma}(E_p)=10n_{sp}\omega\left[\frac{1}{2}\mathcal{N}_h\left(1-\frac{\gamma}{5}-\frac{2}{5}n_{sp}E_h\right)+n_{sp}(E_p-E_d)+\frac{1}{10}n_{sp}^2E_p^2+N_h^{\sigma}\left(1+\frac{1}{5}n_{sp}(E_p-E_h^{\sigma})\right)\right]. \quad (6)$$

In a square-band model, assuming that the Fermi level crosses both d bands, Eq. (6) holds for $E_p \geqslant W_d(1+N_h^-/5)$. In particular, it is relevant for $5 \leqslant E_p \leqslant 10\,\mathrm{eV}$, which is precisely the energy domain investigated in Ref. 16. It can be written in a form analogous to Eq. (1) after substituting the relations $\mathcal{N}_h=2N_h^{\sigma}+\sigma\Delta\mathcal{N}_h$ and $N_h^{\sigma}E_h^{\sigma}=(\frac{1}{2})(\mathcal{N}_hE_h-\sigma\Delta\mathcal{N}_hE_h')$. By this way, we identify terms proportional to N_h^{σ}, as in Eq. (1), but also terms proportional to $\Delta\mathcal{N}_h$. Introducing proper σ_0, σ_d, and σ_d' coefficients, which are no longer constant (in particular σ_d and σ_d' depend on the γ factor), we obtain

$$\frac{R^{\pm}}{v}=\sigma^{\pm}=\sigma_0+\sigma_dN_h^{\pm}\pm\sigma_d'\frac{\Delta\mathcal{N}_h}{2} \quad (7)$$

v is the electron velocity, taken as proportional to $[E_p+E_F]^{2/3}$ to ensure a constant density of states in the sp band. The Fermi energy E_F specifies the location of the bottom of the sp band. These relations are physically reasonable as both scattering cross sections, for minority- and majority-spin electrons, increase with the hole number. As expected, this arises because, if a majority-spin electron cannot ''fall'' into empty majority-spin d states, it may undergo small energy losses, exciting a minority-spin electron inside the minority-spin d band. Remark that these small energy losses, which are equally possible for up- and down-spin electrons, do not contribute to $\Delta\sigma$, but only to the spin-averaged IMFP. Then,

$$\langle\sigma\rangle=\sigma_0+\sigma_d\frac{\mathcal{N}_h}{2}, \quad (8)$$

$$\Delta\sigma=(\sigma_d-\sigma_d')\Delta\mathcal{N}_h, \quad (9)$$

$$A=\frac{\Delta\sigma}{2\langle\sigma\rangle}=\frac{1}{4}\frac{\Delta\mathcal{N}_h}{(\sigma_0/\sigma_d)+\frac{\mathcal{N}_h}{2}}\frac{1+\frac{1}{5}n_{sp}(E_p-E_h')}{1-\frac{\gamma}{10}+\frac{1}{10}n_{sp}(E_p-3E_h)}. \quad (10)$$

For a material with a small hole number and at moderate primary energy, we observe that the Schönhense and Siegmann expressions for $\Delta\sigma$ and A [Eqs. (3) and (4)] are overestimated by a factor of 2. For a strong ferromagnet, Eq. (4) predicts a maximum spin asymmetry $A=100\%$ ($\mathcal{N}_h=\Delta\mathcal{N}_h=N_h^-$, $\sigma_0=0$), whereas Eq. (10) yields $A\approx 50\%$. This important result can be simply understood as follows. The main contributions to the scattering cross section originate from processes involving several d states. In the energy domain that we consider, the relevant events involve two d states and are of two types:

(i) A primary electron with a spin $\pm$ falls into the empty d states of same spin, undergoing a large energy loss, and excites an electron with either spin from the occupied d states or into the empty d states. Such events contribute to the scattering rate proportionally to $N_h^{\pm}(N_h^++N_e^++N_h^-+N_e^-)=10N_h^{\pm}$, where $N_e^{\pm}=(5-N_h^{\pm})$ is the number of electrons with a spin $\pm$ in the d bands. We refer to this contribution as $\sigma_d^*N_h^{\pm}$; it corresponds to the N_h^{σ} term in Eq. (6) and is responsible for the spin asymmetry of the scattering cross section.

(ii) A primary electron loses a small energy amount and excites an electron with either spin from the occupied d states into the empty d states. The corresponding contribution is proportional to $N_h^+N_e^++N_h^-N_e^-=5\mathcal{N}_h(1-\gamma/5)$. We refer to this contribution as $\sigma_d'\mathcal{N}_h/2$; it corresponds to the $\mathcal{N}_h$ term in Eq. (6) and does not contribute to the spin asymmetry of the scattering cross section.

The overall contribution of the (i) and (ii) events to the scattering rate is $\sigma_d^*N_h^{\pm}+\sigma_d'\mathcal{N}_h/2=(\sigma_d^*+\sigma_d')N_h^{\pm}\pm\sigma_d'\Delta\mathcal{N}_h/2$, to be compared to Eq. (7). σ_d^* and σ_d' have now a simple physical meaning as they respectively express the contribution to the scattering cross section of the transitions with large and small amounts of energy transfer. Obviously, we have $\Delta\sigma=\sigma_d^*\Delta\mathcal{N}_h$ and $\sigma_d=\sigma_d^*+\sigma_d'$. If all the transition matrix elements are equal, $\sigma_d/\sigma_d^*=2(1-\gamma/10)$, which explains the main terms in Eq. (10). On the contrary, in the Schönhense and Siegmann model where the transitions involving small energy transfers are overlooked ($\sigma_d'=0$), it is incorrectly concluded that $\sigma_d/\sigma_d^*=1$. From this analysis, it appears that fitting experimental A values through Eq. (4), leads to increase the (σ_0/σ_d) ratio by a $\mathcal{N}_h$-dependent factor larger than 2 (3.3 for Co and 4.1 for Fe), whereas a constant value of about 3.6, providing a good numerical fit, is used in Ref. 16.

C. A step beyond

Whereas the preceding model gives an insight in the physics, a precise comparison with experimental data needs more adaptability, coming through the relative weight of the different transitions, an approach related to the careful analysis of Ref. 19. For that, we perform the R^{σ} calculation, step by step following the procedure described in Ref. 17, but just performing the integration on the amount of energy loss ε after cutting the domain in *three* parts: from 0 to W (A domain), from W to E_M (B domain), and from E_M up to E_p (C domain); E_M is a somewhat arbitrary cutoff energy which verifies $E_p-E_M \geqslant \sup(0,E_2^+,E_2^-)$. In such a model, the electrons are treated as distinguishable particles, which appears to be a reasonable approximation in the energy range we consider [a justification is given in Ref. 19. There, in Appendix A, Eq. (A1), the cross terms in the first matrix element are neglected, which is equivalent to ignore the wavefunction antisymmetrization. This approximation is further discussed in Sec. III of Ref. 19 and is based on the numerical results of Ref. 4]. The matrix elements are assumed to depend only on the (s or d) nature of the states involved, in each given energy domain. Both spin channels are treated on an equal footing. To track the origin of the different terms,

we refer to the weight of a transition between k and k' states (where $k=s$ or p) by introducing the factor $\omega_{kk'}$ in the calculation. At the end, to make the link with the notations of Ref. 19, weperform the identification $\omega_{ss}\omega_{ss}=(2\pi/\hbar)|M_{ss}^{ss}|^2$, $\omega_{ss}\omega_{sd}=(2\pi/\hbar)|M_{ss}^{sd}|^2$, $\omega_{sd}\omega_{sd}=(2\pi/\hbar)|M_{ds}^{sd}|^2$, $\omega_{ss}\omega_{dd}=(2\pi/\hbar)|M_{sd}^{sd}|^2$ (the superscript indicates the nature of the initial states, the subscript, the nature of the final states). These matrix elements are *proportional* to the Coulomb matrix elements (they should include a factor accounting for the ion density; an estimate of this low-energy matrix elements is extremely difficult because of the importance of screening). A straightforward calculation yields the following expression, which is a natural extension of Eq. (6):

$$\frac{R^\sigma}{10n_{sp}(2\pi/\hbar)}=\frac{1}{2}\mathcal{N}_h\left[\left(1-\frac{\gamma}{5}\right)|M_{sd}^{sd}(A)|^2-\frac{2}{5}n_{sp}E_h|M_{ss}^{sd}(A)|^2\right]+n_{sp}(W-E_d)|M_{ss}^{sd}(A)|^2+\frac{1}{10}n_{sp}^2W^2|M_{ss}^{ss}(A)|^2$$
$$+n_{sp}(E_M-W)|M_{ss}^{sd}(B)|^2+\frac{1}{10}n_{sp}^2(E_M^2-W^2)|M_{ss}^{ss}(B)|^2+n_{sp}(E_p-E_M)|M_{ss}^{sd}(C)|^2+\frac{1}{10}n_{sp}^2$$
$$\times(E_p^2-E_M^2)|M_{ss}^{ss}(C)|^2+N_h^\sigma\left[|M_{ds}^{sd}(C)|^2+\frac{1}{5}n_{sp}(E_p-E_h^\sigma)|M_{ss}^{sd}(C)|^2\right]. \tag{11}$$

The indications (A), (B), or (C) refer to the energy domain where the matrix element has to be evaluated. An important conclusion is that the energy dependence of $\Delta\sigma$ directly reflects the $|M_{ds}^{sd}|$ exchange-matrix-element energy dependence. In Ref. 19, it is empirically concluded that the cascade polarization value, or equivalently the IMFP asymmetry (see Sec. 2 of the Appendix), is not sensitive to the $|M_{sd}^{sd}|^2/|M_{ss}^{sd}|^2$ ratio, which is not true in general, and the variation of the squared exchange matrix element is approximated by the law $[1+(\varepsilon/B)^2]^{-1}$, where ε is the energy transfer. For simplicity, we only retain the energy dependence of the exchange matrix element, which is expected to fall off much faster with increasing energy.[19] Then, the whole energy dependence contained in the matrix elements is restricted to the $|M_{ds}^{sd}(C)|$ term, which will be evaluated at E_p and referred to as $|M_{ds}^{sd}(E_p)|$. In the terms proportional to the hole numbers, the domain indication will be kept in the $|M_{ss}^{sd}|$ matrix elements only to recall the origin of these contributions. This also allows us to keep the full energy dependence of $\Delta\sigma$. In the absence of domain indication, the matrix elements are evaluated in the A region. Consequently,

$$\frac{R^\sigma}{10n_{sp}(2\pi/\hbar)}=\mathcal{N}_h\left[\frac{1}{2}\left(1-\frac{\gamma}{5}\right)|M_{sd}^{sd}|^2-\frac{1}{5}n_{sp}E_h|M_{ss}^{sd}|^2\right]$$
$$+n_{sp}(E_p-E_d)|M_{ss}^{sd}|^2+\frac{1}{10}n_{sp}^2E_p^2|M_{ss}^{ss}|^2$$
$$+N_h^\sigma\left[|M_{ds}^{sd}(E_p)|^2\right.$$
$$\left.+\frac{1}{5}n_{sp}(E_p-E_h^\sigma)|M_{ss}^{sd}(E_p)|^2\right]. \tag{12}$$

As in Sec. II B [Eq. (7)], we can calculate σ_0, σ_d, and σ_d', or equivalently σ_0, σ_d, and $\Delta\sigma$. Assuming that the matrix elements do not depend on the material considered, a simplifying assumption which may be rather intuitive in a rigid band model, we see in the above expressions that the E_d, E_h, and E_h' terms [the two latter arising from the $N_h^\sigma E_h^\sigma$ product, see the derivation of Eq. (7)], generally smaller than W_d, still contain some material dependence. In usual cases, they can alternatively be viewed as related to the hole numbers: in a square d-band model and assuming that the Fermi level crosses both bands (obviously, the results will hold if the Fermi level is not far from the d bands, the energy scale being their energy width W_d) it is readily shown that $E_h=\gamma W_d/10$ and $E_h'=\mathcal{N}_hW_d/10$, $E_d=E_d^0-\mathcal{N}_hW_d/10$, where E_d^0 is the spin-averaged center of the d bands if both d bands are completely full. Concerning E_d, we also observe that the expression holds whatever the d-band shape, in the extreme case where each d band is either completely full or empty. The validity of this linear approximation in real cases is supported by the calculation given in Ref. 20 (Fig. 2, p. 22). *In the following (except when $\mathcal{N}_h=0$) we will retain these expressions* and we observe that $2n_{sp}E_F=\mathcal{N}_e^{sp}$, where $\mathcal{N}_e^{sp}$ is the electron number in the sp band, which appears to be of the order of unity, due to s-d transfer.[20] This means that the ratio of the densities of states in the sp to the d bands is about $n_{sp}W_d/5=(1/10)(W_d/E_F)\mathcal{N}_e^{sp}$, i.e., of the order or smaller than 0.1. We write

$$\sigma_0=\frac{v_F}{v}\sigma_d^0\varrho_0, \tag{13}$$

$$\sigma_d=\frac{v_F}{v}\sigma_d^0\varrho_d, \tag{14}$$

where v_F is the electron velocity at the Fermi level and

$$\sigma_d^0=\left(\frac{n_{sp}}{v_F}\frac{2\pi}{\hbar}|M_{ds}^{sd}|^2\right) \tag{15}$$

and we obtain

$$\varrho_0 = 5\mathcal{N}_e^{sp}\left[\frac{E_p - E_d^0}{E_F}\frac{|M_{ss}^{sd}|^2}{|M_{ds}^{sd}|^2} + \frac{1}{20}\mathcal{N}_e^{sp}\left(\frac{E_p}{E_F}\right)^2\frac{|M_{ss}^{ss}|^2}{|M_{ds}^{sd}|^2}\right], \tag{16}$$

$$\varrho_d = \mathcal{N}_e\left(1 - \frac{\Delta\mathcal{N}_h^2}{\mathcal{N}_e\mathcal{N}_h}\right)\left[\frac{|M_{sd}^{sd}|^2}{|M_{ds}^{sd}|^2} + \frac{\mathcal{N}_e^{sp}}{10}\frac{W_d}{E_F}\frac{|M_{ss}^{sd}|^2}{|M_{ds}^{sd}|^2}\right] + 10\left[\frac{|M_{ds}^{sd}(E_p)|^2}{|M_{ds}^{sd}|^2} + \frac{\mathcal{N}_e^{sp}}{10}\left(\frac{E_p}{E_F} - \frac{\gamma}{10}\frac{W_d}{E_F}\right)\frac{|M_{ss}^{sd}(E_p)|^2}{|M_{ds}^{sd}|^2}\right], \tag{17}$$

$$\Delta\sigma = \left[10\frac{|M_{ds}^{sd}(E_p)|^2}{|M_{ds}^{sd}|^2} + \mathcal{N}_e^{sp}\left(\frac{E_p}{E_F} - \frac{\mathcal{N}_h}{10}\frac{W_d}{E_F}\right)\frac{|M_{ss}^{sd}(E_p)|^2}{|M_{ds}^{sd}|^2}\right]\frac{v_F}{v}\sigma_d^0\Delta\mathcal{N}_h, \tag{18}$$

where $\mathcal{N}_e = 10 - \mathcal{N}_h$ is the number of electrons in the d bands. In the ϱ_d expression, the following relations have been used:

$$\gamma = \frac{\mathcal{N}_h}{2} + \frac{\Delta\mathcal{N}_h^2}{2\mathcal{N}_h}, \tag{19}$$

$$1 - \frac{\gamma}{5} = \frac{1}{10}\mathcal{N}_e\left[1 - \frac{\Delta\mathcal{N}_h^2}{\mathcal{N}_e\mathcal{N}_h}\right]. \tag{20}$$

$\Delta\mathcal{N}_h^2/\mathcal{N}_e\mathcal{N}_h$ is zero for a nonferromagnetic material and is much smaller than unity for materials with small or large hole numbers and can sometimes be neglected. When $\mathcal{N}_h = 0$, because the top of the d bands may be located significantly below the Fermi level, E_d has to be kept in the ϱ_0 expression instead of E_d^0. The importance of the terms involving $\mathcal{N}_e^{sp}$ in these expressions depends on the matrix element ratios, which are expected to be larger than unity as the denominator is an exchange-type matrix element.[19]

These results have been derived assuming a constant density of states n_{sp} in the sp band. This is reasonable for $E_p \leqslant E_F$. For larger E_p, it is more realistic to cut this density of states below the energy $-E_F$ through a multiplication by a Heaviside function. Here again the calculation is straightforward, assuming $E_F \geqslant W$, in the domain $E_p \geqslant E_F + 2\sup(0, E_2^+, E_2^-)$. In a square band model, this condition implies that $E_p \geqslant E_F + 2N_h^- W_d/5$. In the calculation of R^σ, we perform the integration on the amount of energy loss ε after cutting the domain at energies W, E_F, $E_F + \sup(0, E_2^{\pm\sigma})$ for direct (involving the $+\sigma$ channel) and exchangelike (involving the $-\sigma$ channel) processes, E_M, and E_p [with $E_p - E_M \geqslant \sup(0, E_2^+, E_2^-)$]. We obtain the important relations

$$\frac{R^\sigma}{10 n_{sp}(2\pi/\hbar)} = \mathcal{N}_h\left[\frac{1}{2}\left(1 - \frac{\gamma}{5}\right)|M_{sd}^{sd}|^2 - \frac{1}{10}n_{sp} \times (E_p + E_h - E_F)|M_{ss}^{sd}|^2\right] + n_{sp}(E_p - E_d)|M_{ss}^{sd}|^2 + \frac{1}{5}n_{sp}^2 E_F \times \left(E_p - \frac{1}{2}E_F\right)|M_{ss}^{ss}|^2 + N_h^\sigma\left[\left(1 - \frac{\mathcal{N}_h}{10}\right)|M_{ds}^{sd}(E_p)|^2 + \frac{1}{5}n_{sp}E_F|M_{ss}^{sd}(E_p)|^2\right], \tag{21}$$

$$\varrho_0 = 5\mathcal{N}_e^{sp}\left[\frac{(E_p - E_d^0)}{E_F}\frac{|M_{ss}^{sd}|^2}{|M_{ds}^{sd}|^2} + \frac{1}{10}\mathcal{N}_e^{sp}\left(\frac{E_p}{E_F} - \frac{1}{2}\right)\frac{|M_{ss}^{ss}|^2}{|M_{ds}^{sd}|^2}\right], \tag{22}$$

$$\varrho_d = \mathcal{N}_e\left(1 - \frac{\Delta\mathcal{N}_h^2}{\mathcal{N}_e\mathcal{N}_h}\right)\frac{|M_{sd}^{sd}|^2}{|M_{ds}^{sd}|^2} + \mathcal{N}_e\frac{|M_{ds}^{sd}(E_p)|^2}{|M_{ds}^{sd}|^2} + \mathcal{N}_e^{sp}\frac{2E_F + (1 - 0.1\gamma)W_d - E_p}{E_F}\frac{|M_{ss}^{sd}|^2}{|M_{ds}^{sd}|^2}, \tag{23}$$

$$\Delta\sigma = \left[\mathcal{N}_e\frac{|M_{ds}^{sd}(E_p)|^2}{|M_{ds}^{sd}|^2} + \mathcal{N}_e^{sp}\frac{|M_{ss}^{sd}(E_p)|^2}{|M_{ds}^{sd}|^2}\right]\frac{v_F}{v}\sigma_d^0\Delta\mathcal{N}_h. \tag{24}$$

In Eq. (21), the energy domain where $|M_{ss}^{sd}|^2$ has to be evaluated is only indicated in the term proportional to N_h^σ. This leads to a simpler expression, whereas the full matrix-element energy dependence is kept in Eq. (24). Note that the main features of Eq. (21) are quite intuitive. Indeed, the contribution to the scattering cross section of the transitions involving a large energy transfer [the (i) events in the discussion of Sec. II B] is now proportional to $N_h^\pm(N_e^+ + N_e^-) = N_h^\pm\mathcal{N}_e$, because the excitation of electrons from the sp band into the empty d states is no longer possible.

III. COMPARISON WITH EXPERIMENT

In the framework of the model derived in Sec. II C, we now analyze experimental data found in the literature. Table I summarizes the material parameters which will be useful in the following. To allow a simple comparison with the results of Ref. 16, the electron and hole numbers given in line b will be used. The results are not very sensitive to the $\mathcal{N}_e^{sp}$, W_d, and E_F values so that, for simplicity, we take $\mathcal{N}_e^{sp} = 1$ and $W_d = 5$ eV (except for the specific case of Gd, where the value $\mathcal{N}_e^{sp} = 2$ will also be considered). We retain approximate values of the E_F parameter, which specifies the constant density of states used to schematize the sp band and defines its low-energy end: in Sec. III A, where we study $\Delta\sigma$ in Co and Fe, we take $E_F = 8$ eV; in Sec. III B, where we compare all the materials listed in Table I, we use the average value $E_F = 7$ eV (except when stated in the discussion of

TABLE I. Parameters of the materials considered in Sec. III. The crystal structure referring to these data is indicated in column 1. The values of $\mathcal{N}_e$, $\mathcal{N}_e^{sp}$, $\mathcal{N}_h$, and $\Delta\mathcal{N}_h$ indicated in line *a* (*b*) are taken from Ref. 20 (Ref. 16). The atomic concentration is after Ref. 15. The E_F value (defining the energy location of the bottom of the *sp* band, at energy $-E_F$) given in line *a* is an estimate after Ref. 20. The value indicated in line *b* is calculated in a free electron model, $E_F=\hbar^2k_F^2/2m$, i.e., $E_F(\mathrm{eV})\approx 1.7[d(10^{22}\,\mathrm{cm}^{-3})\mathcal{N}_e^{sp}]^{2/3}$, m being the free-electron mass and k_F the Fermi wave vector, related to the atomic concentration d through the relation $k_F^3=3\pi^2 d\mathcal{N}_e^{sp}$. The E_F value indicated in line *c* is calculated in a model were the *sp* density of states is a constant, which implies that E_F is proportional to k_F^3; the 5.6-eV value of line *b* has been kept for Au and the other values have been deduced from the $d\,\mathcal{N}_e^{sp}$ product. The W_d values are rough estimates after Ref. 20. The γ value is calculated with the hole and electron numbers given in line *b*. E_d is a rough estimate after Ref. 20 for metals with $\mathcal{N}_h=0$.

		Atomic configuration	$\mathcal{N}_e$	$\mathcal{N}_e^{sp}$	$\mathcal{N}_h$	$\Delta\mathcal{N}_h$	Cocentration $\times 10^{22}\,\mathrm{cm}^{-3}$	E_F (eV)	W_d (eV)	γ	E_d (eV)
Cr	*a*	$3d^5 4s^1$	4.96	1.04	5.05	0	8.33	8.0	7.1	2.50	
bcc	*b*		5		5	0		7.2			
	c							7.4			
Fe	*a*	$3d^6 4s^2$	6.93	1.07	3.07	2.25	8.50	8.6	5.5	2.31	
bcc	*b*		7		3	2.2		7.4			
	c							7.8			
Co	*a*	$3d^7 4s^2$	7.87	1.13	2.13	1.75	8.97	8.9	4.8	1.70	
hcp	*b*		8.2		1.8	1.7		8.0			
	c							8.7			
Ni	*a*	$3d^8 4s^2$	8.97	1.03	1.03	0.67	9.14	9.5	4.9	0.50	
fcc	*b*		9.5		0.5	0.5		7.6			
	c							8.0			
Cu	*a*	$3d^{10} 4s^1$	9.91	1.09	0.09	0	8.45	9.5	3.7	0	4.2
fcc	*b*		10		0	0		7.5			
	c							7.9			
Ag	*a*	$4d^{10} 5s^1$	10	1.00	0	0	5.85	7.2	3.5	0	4.7
fcc	*b*		10		0	0		5.5			
	c							5.0			
Gd	*a*	$5d^1 6s^2$					3.02			4.52	
hcp	*b*		1	2	9	0.54		5.6			
	c							5.2			
Ta	*a*	$5d^3 6s^2$	3.78	1.21	6.22	0	5.55	7.4	10	3.50	
bcc	*b*		3		7	0		5.3			
	c							5.7			
Au	*a*	$5d^{10} 6s^1$	9.89	1.11	0.11	0	5.90	10	5.7	0	3.7
fcc	*b*		10		0	0		5.6			
	c							5.6			

the Gd case, where we take $E_F=5.5$ eV); in Sec. III C, where we compare cascade polarization values, we take $E_F=8$ eV for Fe, Co, Ni, and $E_F=5.5$ eV for Gd; in Sec. III D, the spin-averaged IMFP is analyzed with $E_F=5.5$ eV for Au, Ag, and Gd, and $E_F=8$ eV for Fe and Co. For materials with $\mathcal{N}_h\neq 0$, we take $E_d^0=W_d/2=2.5$ eV whereas otherwise we use $E_d=4$ eV.

A. σ_d^0 determination

The spin-dependent IMFP component can be measured with accuracy (see the Appendix), and, as it mostly originates from the electron-electron interaction involving *d* electrons, it can be precisely compared to the model predictions. In fact, some spin asymmetry may also arise from other interactions,[6] especially the interaction with plasmons,[21] but in this case, the corresponding spin-dependent scattering cross section should be a minute fraction of the scattering cross section due to the interaction with plasmons. We will show that the latter is small compared to the scattering cross section due to electron-electron scattering involving the *d* bands (at least in the energy domain where the spin asymmetry is significant). In the case of Co thin films, $\Delta\sigma$ measurements as a function of E_p are reported in Ref. 13 and lower energy measurements giving higher values ($\Delta\sigma\approx 0.8\,\mathrm{nm}^{-1}$ at 1.7 eV), obtained through a probably more reliable technique (see Sec. 3 of the Appendix), have been reported in Ref. 22. The mean free path of majority- and minority-spin electrons in Co was measured at several energies in Refs. 6 and 23 and this allows us to calculate $\Delta\sigma$ values. Similar measurements were performed in Fe.[23,24] A compilation of all these data is presented in Fig. 2; the Fe

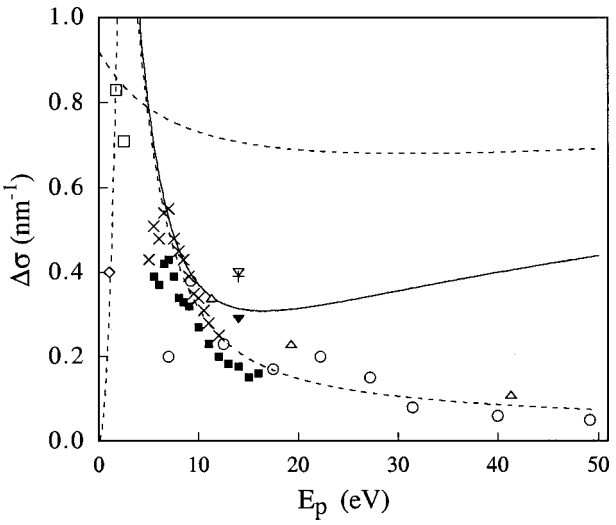

FIG. 2. $\Delta\sigma$ in Co. The dark squares and crosses are data from Ref. 13 (■, 2.5-nm-thick layer, ×, 4-nm-thick layer), the circles (○) from Ref. 6, the squares (□) from Ref. 22, the diamond from Ref. 25. The triangles (△) have been measured in Ref. 24 for Fe and the values have been multiplied by $\Delta\mathcal{N}_h(\mathrm{Co})/\Delta\mathcal{N}_h(\mathrm{Fe})=0.77$. The (▽) and (+) points, taken from Ref. 23, respectively refer to Fe (multiplied by 0.77) and Co, on a W substrate; the (▼) point refers to Fe (multiplied by 0.77) on a Cu substrate. In the calculations, the values $E_F=8$ eV, $W_d=5$ eV, $\mathcal{N}_e^{sp}=1$ are used. The dotted parabola is the low-energy variation [Eq. (25)] with an overall bracket value equal to 1.5. The full curve is a fit through Eq. (18), valid close to 7 eV. The lowest dotted curve is a fit through Eq. (24), strictly valid above 11 eV. Both fits use a $[1+(E_p/4)^2]$ law to describe the exchange-matrix-element variation. The values $\sigma_d^0=0.044\,\mathrm{nm}^{-1}$ and $|M_{ss}^{ds}|^2/|M_{ds}^{sd}|^2=3.5$ have been chosen. The upper dotted curve is calculated using a constant exchange matrix element, with the 5-eV value of the preceding calculation.

values from Refs. 23 and 24 have been scaled, according to Eqs. (18) and (24), by multiplication by $\Delta\mathcal{N}_h(\mathrm{Co})/\Delta\mathcal{N}_h(\mathrm{Fe})=0.77$. The scaling remains almost exact in the higher energy domain, because the exchange matrix element is negligible; from the analysis which follows, it can bee checked that the Fe points are underestimated by only 5% at 15 eV. To determine the σ_d^0 value in Co, we use Eq. (18) and the data from Ref. 13. For a first estimate, we consider the measurements of $\Delta\sigma$ at $E_p=6$ eV (almost the lowest energy where the model strictly applies, 6.75 eV, see Sec. II B). Because the different samples give somewhat different results and as stray effects will reduce the spin asymmetry, we use the largest values and take $\Delta\sigma(\mathrm{Co})=0.50\,\mathrm{nm}^{-1}$. Neglecting the term proportional to $\mathcal{N}_e^{sp}$ in Eq. (18) and taking $|M_{ds}^{sd}(6\,\mathrm{eV})|^2/|M_{ds}^{sd}|^2=1$, we obtain $(v_F/v)\sigma_d^0\approx 0.029\,\mathrm{nm}^{-1}$, i.e., $\sigma_d^0\approx 0.043\,\mathrm{nm}^{-1}$. At $E_p=15$ eV, $\Delta\sigma$ is strongly reduced, being of the order of 0.15 nm^{-1}: assuming that the exchange matrix element at this energy is small, we deduce from Eq. (24) $|M_{ss}^{sd}(15\,\mathrm{eV})|^2/|M_{ds}^{sd}|^2\leqslant 4.2$. The $\sigma^{\pm}$ values measured in Fe in Ref. 24 keep a sizable asymmetry at $E_p=41$ eV, where $\Delta\sigma\approx 0.1\,\mathrm{nm}^{-1}$. Using the σ_d^0 value determined for Co and assuming that $|M_{ds}^{sd}(41\,\mathrm{eV})|^2=0$, with Eq. (24), we find $|M_{ss}^{sd}(41\,\mathrm{eV})|^2/|M_{ds}^{sd}|^2=3.5$. Because at such large energies, a decrease of $|M_{ss}^{sd}(E_p)|^2$ with energy should probably be considered, we conclude that $3.5\leqslant|M_{ss}^{sd}|^2/|M_{ds}^{sd}|^2\leqslant 4.2$, in reasonable agreement with Ref. 19, where a ratio of 7.7 and 5.3 is, respectively, taken for Fe and Ni, to fit experimental data. The origin of the higher values found in Ref. 19 is the following: this ratio also appears in the σ_0 expression so that, if the electron scattering cross section were entirely determined by the electron-electron interaction, as assumed in Ref. 19, an increased σ_0 value would be necessary to calculate IMFP asymmetries which do not significantly exceed the experimental values (see Sec. III C). On the contrary, we evidence in Sec. III D that the interaction with plasmons has also to be considered. In Fig. 2, the fit of the $\Delta\sigma$ variation in the higher-energy part has been obtained through Eq. (24) with $\sigma_d^0=0.044\,\mathrm{nm}^{-1}$, $|M_{ss}^{sd}|^2/|M_{ds}^{sd}|^2=3.5$, and $|M_{ds}^{sd}(E_p)|^2/|M_{ds}^{sd}|^2=[1+(6/B)^2]/[1+(E_p/B)^2]$,[19] with $B=4$ eV. In Ref. 19, the value $B=3$ eV was proposed for Fe; however, as the exchange-matrix-element ratio is set equal to unity at $E_p=6$ eV, the results are not very sensitive to the B value just below and above 6 eV, whereas the higher energy values are almost entirely determined by the $|M_{ss}^{sd}(E_p)|^2/|M_{ds}^{sd}|^2$ term. The fit of the data through Eq. (18) in the 6–8-eV range, the application domain, does not significantly differ, although slightly better. It is thus remarkable that the simple law expressed by Eq. (24) provides an excellent fit of the experimental data in the 6–50-eV range, with the *same* σ_d^0 value for Co and Fe. An exception are two values in Fe and Co at 14 eV determined in Ref. 23, which although consistent together as the two points are almost superimposed, are significantly higher than other determinations. These points refer to bcc Fe and hcp Co on a W substrate. Another determination, from the same reference, for fcc Fe on a Cu substrate gives a significantly lower value (▼). One could wonder whether this discrepancy reveals some dependence on the metal structure, in particular on the electron density. However, it must be remarked that the data of Ref. 6 concern fcc Co on a Cu substrate, the data of Refs. 13 and 22, hcp Co on an Au substrate, and the data of Ref. 24, fcc Fe on a Cu substrate. The perfect consistency of these various measurements indicates that the dependence of $\Delta\sigma$ on the metal structure should not be very important. This conclusion contrasts with the statement made in Ref. 6, ''The complex morphology of the Co films on Cu (111) is a major problem in the determination of the absolute values of the IMFP'' and supports the idea that $\Delta\sigma$ is a much more intrinsic parameter than $\langle\sigma\rangle$. To analyze the lower energy domain, we first assume that the exchange-matrix element is constant at energies below 5 eV, retaining its 5-eV value which corresponds to a 1.27 ratio. The corresponding curve is drawn in Fig. 2 and agrees well with the data from Ref. 22.

For very low energies, we follow the treatment given in Ref. 17, close to the Fermi level. The result may be truly material dependent as it involves the densities of states at the Fermi level. To get a rough idea, we neglect the density of states in the majority-spin band at the Fermi level, we take $n_d^-(0)=5/W_d$, and we assume that n_{sp} is exactly ten times lower. Thus we obtain

$$\Delta\sigma\approx 125\sigma_d^0\frac{v_F}{v}\left(\frac{E_p}{W_d}\right)^2\left[\frac{|M_{dd}^{sd}|^2}{|M_{ds}^{sd}|^2}+\cdots\right]. \qquad (25)$$

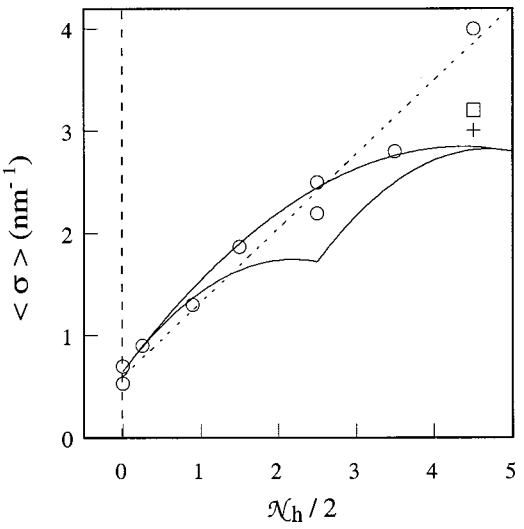

FIG. 3. $\langle\sigma\rangle$ as a function of $\mathcal{N}_h/2$, the spin-averaged hole number. The circles (○) are taken from Ref. 16 and refer to Au and Cu (same point, lowest value), Ag, Ni, Co, Fe, Cr, Ta, and Gd. The square (□) is a plausible value taken from Ref. 27. The dotted line is the linear relation postulated in Ref. 16. The curves have been calculated using the $\underline{\sigma}_d$ expression given in Eq. (17), with $\mathcal{N}_e^{sp}=1$, $W_d=5$ eV, $E_F=7$ eV, and taking $\sigma_0=0.65\,\mathrm{nm}^{-1}$. The upper curve refers to $\gamma=\mathcal{N}_h/2$, the minimum value. The lower curves are calculated for the maximum γ value. The cross (+) has been calculated for Gd at 5 eV with $\mathcal{N}_e^{sp}=2$ and $E_F=5.5$ eV.

The bracket mainly involves transitions within the *d* bands, with the weight $\omega_{sd}\omega_{dd}=(2\pi/\hbar)|M_{dd}^{sd}|^2$, but also a sum of small contributions originating from the $|M_{ds}^{sd}|^2$, $|M_{sd}^{sd}|^2$, $|M_{ss}^{sd}|^2$, and $|M_{ss}^{ss}|^2$ matrix elements. The corresponding parabola is plotted in Fig. 2, with an overall bracket value equal to 1.5. The result is consistent with the data of Filipe *et al.*,[25] who estimate $\Delta\sigma\sim0.4\,\mathrm{nm}^{-1}$ at about 1 eV above the Fermi level in Fe; the corresponding point is indicated in Fig. 2 (diamond). Such a good agreement may be fortuitous since, in bulk Fe, $n_d^+(0)>n_d^-(0)$;[20] however, contrarily to $Fe_{1-x}V_x$ films, Fe layers have not shown an inverted magnetoresistance effect, a possible explanation being that the density of states of ultrathin films may differ from bulk samples.[26] Note that the small experimental decrease of $\Delta\sigma$ just below 6 eV in the data from Ref. 13 is suspicious; moreover, it arises in an energy domain where the IMFP was experimentally found to decrease with decreasing E_p, whereas it should definitely still increase.

B. The spin-averaged scattering cross section in various materials

We now consider the total scattering cross section $\langle\sigma\rangle$ [Eq. (8)]. Figure 3 presents experimental determinations in several materials, for *E_p between 5 and 10 eV*, as a function of $\mathcal{N}_h/2$, after Ref. 16 (○), where these data have been used to postulate a linear relation between the scattering cross section and the hole number (dotted line). In the following analysis, we use Eq. (17), evaluated at $E_p=5$ eV$\sim W_d$ to allow a simple comparison between the various materials, although the model may not strictly apply at this very energy. Taking into account the experimental uncertainties, this is in fact of minor importance. First note that $\underline{\sigma}_d$ presents nonlinear terms as a function of the hole numbers, contained in the γ factor [Eq. (19)]. The minimum γ value, $(\frac{1}{2})\mathcal{N}_h$, is obtained when $\Delta\mathcal{N}_h=0$, i.e., $N_h^+=N_h^-=(\frac{1}{2})\mathcal{N}_h$. This is the case for a nonferromagnetic material. The highest γ value is achieved when $\Delta\mathcal{N}_h$ is maximum. For $\mathcal{N}_h\leqslant5$, in a strong ferromagnet, $N_h^+=0$, $N_h^-=\mathcal{N}_h$ so that $\Delta\mathcal{N}_h=\mathcal{N}_h$ and $\gamma=\mathcal{N}_h$. For $\mathcal{N}_h\geqslant5$, the maximum γ value is obtained when N_h^+ is as low as possible. Thus we have $N_h^-=5$, $N_h^+=\mathcal{N}_h-5$ and $\Delta\mathcal{N}_h=\mathcal{N}_e$. For $E_p\sim W_d$, as the terms proportional to $\mathcal{N}_e^{sp}$ lead to a contribution to $\langle\sigma\rangle$ smaller than 30%, $\underline{\sigma}_d$ takes a simple expression versus hole and electron numbers:

$$\underline{\sigma}_d\approx10+\mathcal{N}_e\left(1-\frac{\Delta\mathcal{N}_h^2}{\mathcal{N}_e\mathcal{N}_h}\right)\frac{|M_{sd}^{sd}|^2}{|M_{ds}^{sd}|^2}. \tag{26}$$

In Fig. 3, the full curves have been calculated and plotted for these extreme γ values. In the calculation, we have used the matrix-element ratios determined in the preceding section, $\sigma_d^0=0.044\,\mathrm{nm}^{-1}$, the value determined in Co, taking $\sigma_0=0.65\,\mathrm{nm}^{-1}$ (very close to the value chosen in Ref. 16), and assuming $|M_{sd}^{sd}|^2/|M_{ds}^{sd}|^2=1.5$. This last ratio, probably larger than unity, cannot reasonably exceed 2: in Fig. 3, the three intercepts of the curves (at $\mathcal{N}_h=0$, 5, and 10) remain fixed whereas the curvature increases when increasing $|M_{sd}^{sd}|^2/|M_{ds}^{sd}|^2$ (note that the Schönhense and Siegmann model corresponds to the case $|M_{sd}^{sd}|^2/|M_{ds}^{sd}|^2=0$; see the discussion in Sec. II B). Here again, this conclusion is consistent with the analysis of Ref. 19, where a (somewhat arbitrary) ratio of 2.3 is taken in Fe and 1.5 in Ni. The overall good agreement with the experimental data demonstrates that the material dependence which could be contained in σ_d^0 is of secondary importance, comforting the picture of a rigid band model. The full curves limit the $\langle\sigma\rangle$ variation domain and we observe that, at a given total hole number, shifting from the lower curves to the upper one corresponds to a transition from a ferromagnetic state to a paramagnetic state: the ferromagnetic state is more transparent for electrons and the difference in the spin-averaged cross section is

$$\frac{1}{2}\frac{v_F}{v}\sigma_d^0\Delta\mathcal{N}_h^2\left(\left|\frac{M_{sd}^{sd}}{M_{ds}^{sd}}\right|^2+\frac{\alpha}{20}\mathcal{N}_e^{sp}\frac{W_d}{E_F}\left|\frac{M_{ss}^{sd}}{M_{ds}^{sd}}\right|^2\right), \tag{27}$$

where $\alpha=3$ in the lower-energy domain considered in this section [Eq. (17) where the energy dependence of $|M_{ss}^{sd}|^2/|M_{ds}^{sd}|^2$ has been neglected] and $\alpha=1$ in the higher-energy domain [Eq. (23)]. This effect can be large and, if detected, it would give a direct estimate of the $|M_{sd}^{sd}|^2/|M_{ds}^{sd}|^2$ ratio. Note the interesting case of Gd. Concerning the experimental Gd point marked by a circle in Fig. 3 (data from Paul, Ref. 27, selected in Ref. 16), which does not agrees with the model, it must be realized that it has a very broad error bar, and that Paul only concludes that the IMFP in Gd ''certainly does not exceeds 4 Å at 5 eV.'' [27] Eastman[11] finds the much lower value $\langle\sigma\rangle=1\,\mathrm{nm}^{-1}$. Besides, the above calculation may be inaccurate as $\mathcal{N}_e^{sp}$ is rather 2 than 1, with E_F of the order of 5.5 eV rather than 7 eV;[15,16] the value calculated

with these parameters is indicated in Fig. 3 (+) and lies very close to a plausible experimental value (□) taken from Ref. 27. In Ref. 16, Gd was considered to support the linear $\langle\sigma\rangle$ variation at large $\mathcal{N}_h$ but it appears that this material rather constitutes a counter example: indeed, $\gamma\approx\mathcal{N}_h/2=4.5$, which means that the intra-*d*-band scattering contribution [see Eq. (17)] is almost suppressed, an intuitive result as the *d* bands are almost empty. This means that, according to Eq. (26), σ_d is reduced by a factor of the order of 2.5 compared to materials with low hole numbers. This is even worse at larger energies [see Eq. (23)] as the whole *d*-band contribution is suppressed because large energy transfer involving the *d* bands are no longer possible. This conclusion is strongly supported by the measurements of Ref. 27 where it is observed that $\langle\sigma\rangle$ is almost constant below 10 eV (of the order of 3 nm^{-1} for the upper determinations, in good agreement with the calculation) but, between 10 and 15 eV, drops down to about 2 nm^{-1}. This will be further analyzed in Sec. III D.

C. σ_0 deduced from the polarization cascade

The polarization cascade determines the IMFP asymmetry *A* (see Sec. 2 of the Appendix). As this determination involves an energy domain slightly exceeding the vacuum level energy, we use Eqs. (17) and (18) with the matrix-element ratios determined in Secs. III A and III B and find

$$A=\frac{1}{4}\,\frac{\Delta\mathcal{N}_h\left[1+0.35\mathcal{N}_e^{sp}\dfrac{E_p-0.1\mathcal{N}_h W_d}{E_F}\right]}{\dfrac{\varsigma_0}{20}+\dfrac{\mathcal{N}_h}{4}\left[1+1.5\left(1-\dfrac{\gamma}{5}\right)+0.35\mathcal{N}_e^{sp}\dfrac{E_p+(1-0.3\gamma)W_d}{E_F}\right]}. \tag{28}$$

This equation, where the value $|M_{sd}^{sd}|^2/|M_{ds}^{sd}|^2=1.5$ has been used, can be compared to Eq. (4), referring to the case to $|M_{sd}^{sd}|^2/|M_{ds}^{sd}|^2=0$. For a strong ferromagnet with a small hole number, neglecting the terms proportional to $\mathcal{N}_e^{sp}$ and with $\sigma_0=0$, Eq. (28) yields $A=40\%$ (instead of 100%). The discrepancy between the two models is thus larger than expected in the simplified picture, with equal matrix elements, given in Sec. II B. From Eq. (28), we now evaluate *A* at $E_p=W_d$ (although the model may not strictly apply at this very energy), taking $\sigma_0=0.65\,nm^{-1}$, the value used in Sec. III B, which corresponds to $\varsigma_0=22.4$. We find $A\approx0.23$ for Fe and Co, $A\approx0.10$ for Ni, and $A\approx0.03$ for Gd, in good agreement with the experimental values $A=0.28$, 0.25, 0.09, and 0.04 quoted in Ref. 16. The only discrepancy is a slightly too low *A* value for Fe, which may partly arise from the uncertainty on the number of *d* holes.[13] Almost the same numerical results are obtained with $\mathcal{N}_e^{sp}=0$, which leads to an extremely simple expression. In the case of Ni, the *A* value is very sensitive to the ς_0 value (and thus to E_p) because of the small hole number, so that the experimental *A* value even allows a good ς_0 estimation. Contrarily to Ref. 16, the *same* σ_0 value accounts very well for both the $\langle\sigma\rangle$ and *A* data. From Eq. (16), neglecting the E_p^2 term which should be relatively small, we estimate $\varsigma_0=8.75W_d/E_F\sim5.5$. Thus, to fit the experimental data, the ς_0 value has been increased by a factor of about 4, which cannot be explained by any reasonable tuning of matrix element ratios. We think that this increase is due to an additional contribution, originating in another scattering mechanism, possibly coupling with damped plasmons.[28] Coupling with plasmons was also invoked in Ref. 27 to explain the very short IMFP (less than 10 Å) measured in Cs in the same energy range. In Ref. 29, where the IMFP is calculated from the dielectric function, a discrepancy is found in Au between the calculated value and the Kanter's data.[30] The contributions of elastic scattering, crystal defect scattering, impurity scattering, etc., are invoked. However, mechanisms that are sample dependent should only yield a small contribution, because the various data taken in the literature are really consistent. Hereafter, we will empirically take into account this contribution by including in σ_0 an additional scattering cross section, which certainly introduces some material dependence, even though it is not revealed by the analysis of the data obtained at energies close to the vacuum level (Secs. III B and C).

D. IMFP energy dependence, σ_0 material dependence

We now consider the IMFP variation with energy in several materials. To fit the experimental data, we use the ς_d expressions given in Eqs. (17) and (23), depending on the energy domain. Concerning ς_0, we use an expression deduced from Eq. (22). Indeed Eq. (16) almost does not differ for E_p close to E_F, the energy range where it applies, because Eq. (22) is the tangent to Eq. (16) at $E_p=E_F$. We write

$$\varsigma_0=17.5\mathcal{N}_e^{sp}\frac{(E_p-E_d^0)}{E_F}+a\,\frac{E_p}{E_F}+b. \tag{29}$$

The *a* and *b* coefficients—*which are material dependent*—empirically account for both electron-electron scattering and a possible additional contribution. In the case of noble metals, as discussed in Sec. II C, E_d is used instead of E_d^0. Gold was studied in detail in several papers,[10,30–32] and reliable, often quoted, low-energy data have been measured by Kanter.[30] In Fig. 4(a), the data from Refs. 30 and 31 have been marked respectively by diamonds and squares; data obtained in Ref. 27 on thin films, from polarization analysis, are indicated by circles (these data have been chosen as they match with Kanter's values and, at larger energies, do not significantly differ from other determinations given in the same reference). Very similar IMFP values are reported in Ref. 30 for Ag [vertical bars in Fig. 4(a)]. However, when

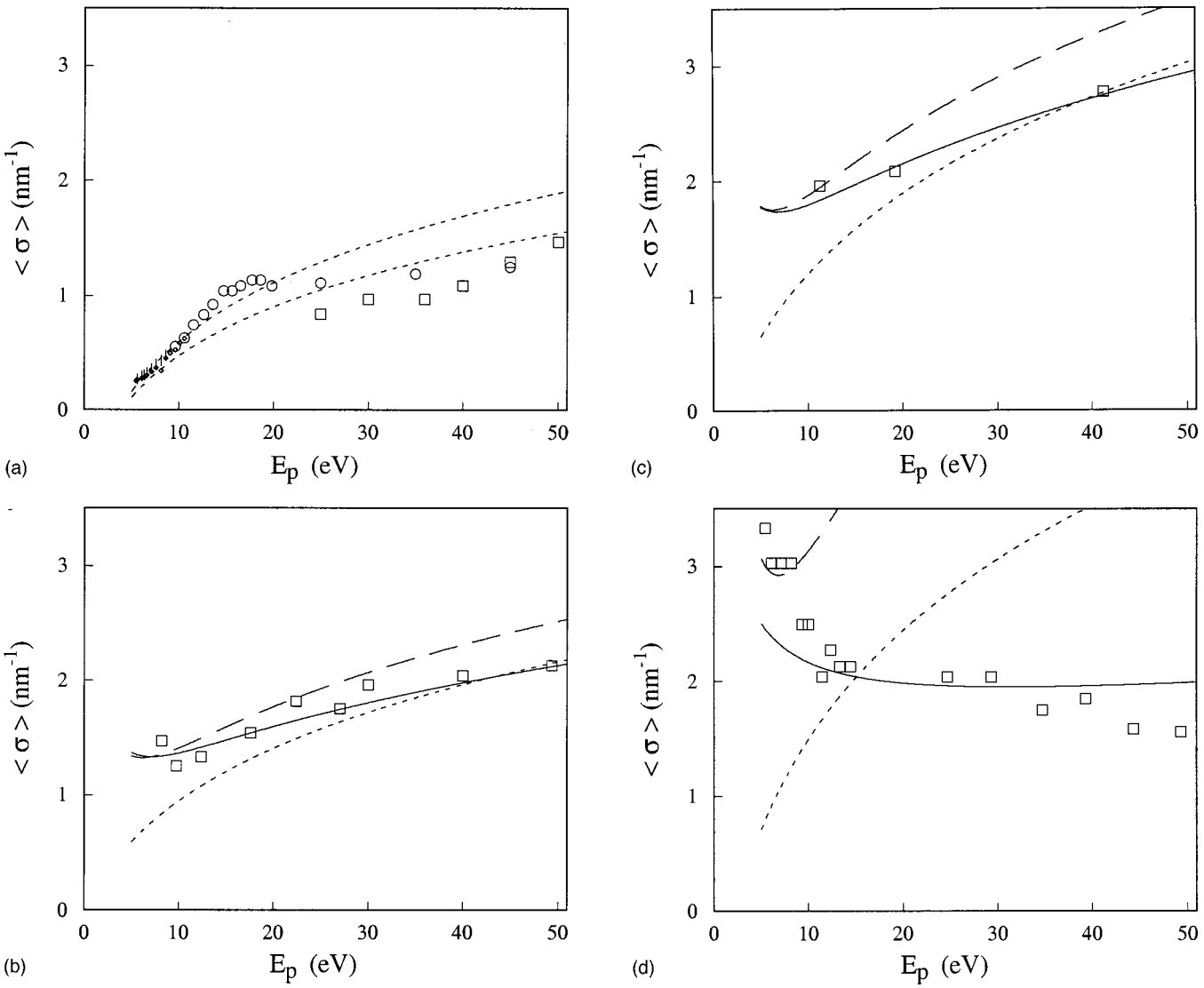

FIG. 4. (a) IMFP in Au and Ag. The small diamonds refer to gold, the vertical bars (|) to Ag, after Ref. 30. The circles (○) are gold values, after Ref. 27, where they have been measured by a technique involving spin-polarized electrons. The squares (□) are gold data, after Ref. 31. The upper dotted curve is a fit through Eq. (29), with $\mathcal{N}_e^{sp}=1$, $E_F=5.5$ eV, $E_d=4$ eV, $a=6$, and $b=-3$. The lower dotted curve has been calculated with $a=1.8$, $b=-0.9$. (b) IMFP in Co. The squares (□) are from Ref. 6. The dotted curve is the σ_0 variation, after Eq. (29) with $\mathcal{N}_e^{sp}=1$, $E_F=8$ eV, $E_d^0=2.5$ eV, $a=11.5$, $b=6$. The dashed curve is a low-energy fit using the σ_d expression given in Eq. (17), valid for $E_p>6.7$ eV. The full curve is a high-energy fit using the σ_d expression given in Eq. (23), valid for $E_p>11.5$ eV. (c) IMFP in Fe. The squares (□) are from Ref. 24. The dotted curve is the σ_0 variation, after Eq. (29) with $\mathcal{N}_e^{sp}=1$, $E_F=8$ eV, $E_d^0=2.5$ eV, $a=24$, $b=0$. The dashed curve is a low-energy fit using the σ_d expression given in Eq. (17), valid for $E_p>7.6$ eV. The full curve is a high-energy fit using the σ_d expression given in Eq. (23), valid for $E_p>13.2$ eV. (d) IMFP in Gd. The squares (□) are from Ref. 27. The dotted curve is the σ_0 variation, after Eq. (29) with $\mathcal{N}_e^{sp}=2$, $E_F=5.5$ eV, $E_d^0=2.5$ eV, $a=12$, $b=-2$. The dashed curve is a low-energy fit using the σ_d expression given in Eq. (17), valid for $E_p>9.8$ eV. The full curve is a high-energy fit using the σ_d expression given in Eq. (23), valid for $E_p>15$ eV.

comparing data from the literature, it must be kept in mind that the IMFP experimental determinations are extremely difficult. For instance, in Ref. 31, the *relative* error in the IMFP determination in gold is estimated to be ±20% whereas the *absolute* IMFP values are assumed to be correct only within ±50%. The fit (upper dotted line) has been obtained with $E_d=4$ eV, $a=6$, and $b=-3$, which, assuming no additional plasmon contribution, corresponds to Eq. (22) with $|M_{ss}^{ss}|^2=3.5|M_{ss}^{sd}|^2$ (and $|M_{ss}^{sd}|^2=3.5|M_{ds}^{sd}|^2$; note that the $|M_{ss}^{ss}|$ matrix element does not appears in Ref. 19 because the occupied *s*-*p* states are not distinguished from the *d*'s). The lower dotted line has been calculated with $|M_{ss}^{ss}|^2 \approx |M_{ss}^{sd}|^2$ ($a=1.8$, $b=-0.9$), which is probably a lower bound because Coulomb matrix elements between *s* and *d* states are presumably smaller than between *s* states, [18] just to visualize the influence of this matrix element ratio. Nevertheless, such a ''good'' agreement (taking into account the uncertainties on the experimental data) may be somewhat fortuitous: as some plasma contribution should certainly be included, the normalizing coefficient for electron-electron scattering, σ_d^0, may be smaller for noble than for 3*d* metals and a compensation may arise from the additional scattering terms. The IMPF values measured in Co, after Ref. 6, are plotted in Fig. 4(b) and the fit is obtained with $a=11.5$, b

$=6$; the Fe data, from Ref. 24 [Fig. 4(c)] are fitted using $a=24$, $b=0$. Figure 4(d) shows the IMFP determined in Gd in Ref. 27 (from polarization analysis, where the results lie between lower and upper bounds determined in the same reference through other techniques). The data are fitted using $a=12$, $b=-2$ [with $E_F=5.5\,\mathrm{eV}$, $\mathcal{N}_e^{sp}=2$]; this a value can be obtained from Eq. (22) with $|M_{ss}^{ss}|^2=1.7|M_{ss}^{sd}|^2$, which should correspond to an upper bound. It spectacularly evidences the scattering cross section *decrease* with increasing energy, due to the suppression of the d-band contributions. The large a values determined in Co and Fe, and the positive b values in Co, Fe, and Gd unambiguously show that the only electron-electron interaction is insufficient to account for the spin-independent part of the IMFP. For Fe, Co, and Gd, the calculation respectively yields σ_0 values at 5 eV equal to 0.65, 0.60, and 0.71 nm^{-1}, which appear to be almost equal, in good agreement with the value $\sigma_0=0.65\,\mathrm{nm}^{-1}$ used in Sec. III B. Noble metals seem to differ, with $\sigma_0\approx 0.16\,\mathrm{nm}^{-1}$ at 5 eV, which suggests that the IMFP values chosen for noble metals in Ref. 16—and reproduced in Fig. 3 of the present paper—rather refer to 10-eV data. The gold value, for instance, is taken from Ref. 27 where it corresponds to a lower bound of the IMFP, which surprisingly remains almost the same for $E_p=10\,\mathrm{eV}$ and $E_p=5$ eV, in contradiction with Kanter's results[30] and with the ''universal law'' generally admitted for noble metals.[2] More detailed investigations, both theoretical and experimental, are necessary for further analysis, but we observe that a good empirical description of the scattering cross sections in the range 5–50 eV is obtained through the very simple laws given by Eqs. (17), (23), and (29). The dotted curves in Figs. 4(b)–4(d) represent the σ_0 variation. They make evident that the picture in which the total scattering cross section consists of a σ_0 part (which, in fact, includes processes involving the d bands) and of a contribution due to the ''scattering by the d holes'' is only pertinent at low energy, close to the vacuum level. A larger energies, the ''d-hole contribution'' even becomes negative!

IV. CONCLUSION

A consistent description of the electron mean free path in transition metals has been given, in the range 5–50 eV. The central result of the present paper is the relation

$$\sigma^{\pm}=\sigma_0+\sigma_d N_h^{\pm}\pm\sigma_d'\frac{\Delta\mathcal{N}_h}{2}$$

which relates the scattering cross section to the hole numbers in the d bands; σ_d and σ_d' originate from the electron-electron interaction. Concerning σ_0 we have shown that an additional contribution has to be included, which probably originates from the coupling with damped plasmons. We have obtained simple expressions of $\Delta\sigma=\sigma^-\sigma^+$ [Eqs. (18) and (24)]and we have shown that direct information on the exchange matrix element can been extracted from its experimental study. It has been established that σ_d is not a constant, but is simply related to the hole and electron numbers [Eq. (26)]. This model accounts for all the presently available experimental data, in particular, the cascade-polarization values and the mean free path values for several materials. The energy variation of the parameters was considered, and the conclusion is that the main effects are a steep decrease of the exchange matrix element and a large increase of σ_0 with energy. For materials with a large hole number, a strong reduction of the spin-averaged scattering cross section $\langle\sigma\rangle=(\sigma^-+\sigma^+)/2$ is predicted—and observed—when E_p exceeds E_F, due to the suppression of the d-band contribution. We have also shown that a metal is always more transparent in a ferromagnetic state than in a paramagnetic state.

ACKNOWLEDGMENTS

I am indebted to J.-P. Boilot, J.-N. Chazalviel, and J. Peretti for fruitful discussions. I thank Catherine Bouton, C. Hermann, G. Lampel, and J. Peretti for a critical reading of the manuscript. This work has been supported by the ''Délégation Générale pour l'Armement.''

APPENDIX: SPIN-DEPENDENT IMFP AND IMFP ASYMMETRY DETERMINATIONS

1. Spin-dependent scattering cross section from the overlayer technique

A well-known technique to determine IMFP's is the overlayer technique in photoemission, in which a ferromagnetic film of controlled thickness x is deposited on to a nonmagnetic substrate. Electrons are injected in the ferromagnetic film, for instance by photoexcitation of a substrate core level.[23,24] Due to a different IMFP for up- and down-spin electrons, a spin polarization is created in the transport process. More generally, if the primary beam has the spin polarization P_0, it is straightforward to show that the spin polarization P_e of the emerging beam is

$$P_e=\frac{a(x)+P_0}{1+a(x)P_0}\approx a(x)+P_0. \tag{A1}$$

Here $a(x)=[t_+(x)-t_-(x)]/[t_+(x)+t_-(x)]$ is the spin asymmetry of the transmission coefficients, expressed as $t_\pm(x)=\exp-(x/\lambda^\pm)$, where λ^- (λ^+) is the IMFP for minority- (majority-) spin electrons. The last equality holds in many cases, where the source polarization and the asymmetry of the transport coefficients are not too high. In Ref. 22, the δ parameter has been defined as follows:

$$\frac{1}{\lambda^-}=\frac{1}{\lambda}+\frac{1}{\delta},$$

$$\frac{1}{\lambda^+}=\frac{1}{\lambda}-\frac{1}{\delta}, \tag{A2}$$

and we have

$$a(x)=\tanh\frac{x}{\delta}. \tag{A3}$$

P_e can also be written

$$P_e=\frac{I^+-I^-}{I^++I^-}, \tag{A4}$$

where $I^{\pm}$ are the emerging currents of up- and down-spin electrons, so that

$$I^{\pm}=\frac{1\pm P_e}{2}I=I_0^{\pm}\exp-\frac{x}{\lambda^{\pm}}. \tag{A5}$$

$I=I^{+}+I^{-}$ is the total emerging current and $I_0^{\pm}$ is the primary current of up- or down-spin electrons. By measuring the emerging intensity and the polarization of the emerging beam versus film thickness, it is possible to deduce $\lambda^{\pm}$. This technique was used in Ref. 13 to determine $\Delta\sigma=2/\delta$ in a transmission geometry, where unpolarized electrons are injected through a freestanding foil. However, in many photoemission experiments, practical problems arise. First, it may happen that the first metal layers grown on the substrate have different magnetic properties.[6] Second, for an increasing metal thickness, polarization measurements become impossible because of the vanishing signal.[6,24] Then, the measurements are restricted to thicknesses of the order of λ. For instance, in Ref. 6, an IMFP of about 0.8 nm is found in Co close to the vacuum level energy whereas it is stated that the more reliable data have been obtained for a metal thickness of 4 monolayers (ML) (1 ML=0.208 nm). To overcome this difficulty, when using an unpolarized primary beam, the mean free path is deduced from the spin-averaged emerging current, which is assumed to determine a spin-averaged IMFP λ_0 in the following way:

$$I^{+}+I^{-}=I_0\exp-\frac{d}{\lambda}\cosh\frac{d}{\delta}=I_0\exp-\frac{d}{\lambda_0}. \tag{A6}$$

We also have

$$I^{\pm}=\frac{I_0}{2}\exp-\frac{d}{\lambda^{\pm}}=\frac{1\pm P_e}{2}(I^{+}+I^{-}) \tag{A7}$$

which yields

$$\frac{1}{\lambda^{\pm}}=\frac{1}{\lambda_0}-\frac{1}{d}\ln(1\pm P_e), \tag{A8}$$

$$\frac{1}{\delta}=\frac{1}{2d}\ln\frac{1+P_e}{1-P_e}, \tag{A9}$$

$$\frac{1}{\lambda}=\frac{1}{\lambda_0}-\frac{1}{2d}\ln(1-P_e^2)=\frac{1}{\lambda_0}+\frac{1}{\delta}-\frac{1}{d}\ln(1+P_e). \tag{A10}$$

In the small metal-thickness regime ($d\ll\delta$), P_e is small and we have $\lambda_0\approx\lambda$. For Co at low energy, we may have $A\sim0.5$, i.e., $\lambda^{+}\sim3\lambda^{-}$, thus $\delta\sim2\lambda$, and we are in this regime for d (notably) smaller than 1.5 nm. In the large metal thickness regime ($\delta\ll d$), we find, as expected, $\lambda_0\approx\lambda^{+}$.

When *spin-polarized* electrons with a $\pm P_0$ spin polarization are injected through a ferromagnetic film, referring to the total transmitted current as $I(\pm P_0)$, we see that

$$\frac{I(+P_0)-I(-P_0)}{I(+P_0)+I(-P_0)}=P_0a(x). \tag{A11}$$

Thus a transmission experiment performed with spin-polarized electrons also determines $a(x)$.[33]

2. IMFP asymmetry from the cascade polarization

When high-energy (a few keV) unpolarized electrons are injected into a ferromagnetic substrate, due to the secondary-electron cascade, a source distribution is formed with a spin polarization P_0 reflecting the bulk magnetization. If one assumes that spin-polarized electrons are uniformly excited in the sample, the numbers of emitted electrons with up and down spin are respectively proportional to

$$\int_0^{\infty}(1+P_0)\exp-(x/\lambda^{+})dx=(1+P_0)\lambda^{+},$$

$$\int_0^{\infty}(1-P_0)\exp-(x/\lambda^{-})dx=(1-P_0)\lambda^{-} \tag{A12}$$

so that the emitted polarization, referred to as the cascade polarization P_c is

$$P_c=\frac{A+P_0}{1+AP_0}\approx A+P_0, \tag{A13}$$

where A is the IMFP asymmetry. With this technique, contrarily to techniques based on ballistic electrons, there is no doubt that the detected electrons have interacted with the ferromagnetic layer. The cascade polarization yields a good estimate of the IMFP asymmetry, averaged within a few eV above the vacuum level energy.

3. IMFP spin dependence from electron transmission through ferromagnetic bilayers

The preceding techniques require to use either a primary spin-polarized electron beam (and to detect the transmitted intensity as a function of the source polarization) or to detect the transmitted-beam polarization. The ferromagnetic-bilayer technique[22] allows us to determine accurately δ, even using an unpolarized electron beam and without any polarization measurement. It makes full use of the ''spin-filter'' concept: a ferromagnetic layer is an electron-spin polarizer. Free electrons are transmitted through an ultrathin *asymmetric ferromagnetic bilayer*, where the ferromagnetic layers may have parallel (''ferromagnetic, *F*'') or antiparallel (''antiferromagnetic, AF'') saturated-magnetization states and, when *unpolarized* electrons are injected in the sample, the experiment looks similar to a current perpendicular-to-plane magnetoresistance (CPP-MR) experiment on a spin valve. Let us consider the ballistic electron transmission of an electron beam through n ferromagnetic layers embedded in nonmagnetic metals. We describe the magnetic configuration of the structure through the n-dimensional $\boldsymbol{\mu}$ configuration vector of components $\mu_i=\pm1$ depending upon whether the majority-spin direction in the ith layer is parallel or antiparallel to the quantization axis. Electrons with spin $\sigma=\pm1$ are transmitted through the sample with a spin-dependent transmission coefficient $t_{\boldsymbol{\mu}\sigma}$. Because the relevant parameter is the relative orientation of the incident spin with respect to the magnetization direction, we have the symmetry relation $t_{\boldsymbol{\mu}\sigma}=t_{-\boldsymbol{\mu}-\sigma}$. The transmitted intensity $I_P(\boldsymbol{\mu})$ expresses as

$$I_P(\boldsymbol{\mu})=(1/2)I[(1+P)t_{\boldsymbol{\mu}^{+}}+(1-P)t_{\boldsymbol{\mu}^{-}}]. \tag{A14}$$

The spin-averaged transmitted intensity $I_0(\boldsymbol{\mu})$, equal to the transmitted intensity when the primary beam is unpolarized, and the spin-dependent part of the transmitted current $\Delta I_P(\boldsymbol{\mu})$, write

$$I_0(\boldsymbol{\mu}) = (1/2)[I_P(\boldsymbol{\mu}) + I_{-P}(\boldsymbol{\mu})] = (1/2)I(t_{\boldsymbol{\mu}+} + t_{\boldsymbol{\mu}-}) = (1/2)[I_P(\boldsymbol{\mu}) + I_P(-\boldsymbol{\mu})], \tag{A15}$$

$$\Delta I_P(\boldsymbol{\mu}) = (1/2)[I_P(\boldsymbol{\mu}) - I_{-P}(\boldsymbol{\mu})] = (1/2)IP(t_{\boldsymbol{\mu}+} - t_{\boldsymbol{\mu}-}) = (1/2)[I_P(\boldsymbol{\mu}) - I_P(-\boldsymbol{\mu})]. \tag{A16}$$

These relations show the equivalence between polarization and magnetization reversal. The transmission asymmetry, i.e., the relative spin dependence of the transmitted current, is

$$\mathcal{A}_P(\boldsymbol{\mu}) = \Delta I_P(\boldsymbol{\mu})/I_0(\boldsymbol{\mu}) = Ps(\boldsymbol{\mu}). \tag{A17}$$

$s(\boldsymbol{\mu}) = (t_{\boldsymbol{\mu}+} - t_{\boldsymbol{\mu}-})/(t_{\boldsymbol{\mu}+} + t_{\boldsymbol{\mu}-})$, the spin asymmetry of the transmission coefficients, analogous to the Sherman function used in spin polarimetry, characterizes the discriminating power of the $\boldsymbol{\mu}$ configuration of the multilayer. In principle, $s(\boldsymbol{\mu})$ can be determined from the measurement of $\mathcal{A}_P(\boldsymbol{\mu})$, provided P is known. In other words, an internal spin-polarization measurement must somehow be performed and this implies the use of at least two layers, a polarizer and an analyzer. Let us consider the quantity

$$I_0(\boldsymbol{\mu})^2 - [\Delta I_P(\boldsymbol{\mu})/P]^2 = I_0(\boldsymbol{\mu})^2[1 - s(\boldsymbol{\mu})^2] = I^2 t_{\boldsymbol{\mu}+} t_{\boldsymbol{\mu}-} = I^2 t_{\boldsymbol{\mu}+} t_{-\boldsymbol{\mu}+}. \tag{A18}$$

The overall transmission coefficient is, in an IMFP-like model where no quantum interferences are considered, the product of the transmission coefficient of each layer. As *both* magnetizations of *each* layer appear in the $t_{\boldsymbol{\mu}+} t_{-\boldsymbol{\mu}+}$ product, it does not depend on the $\boldsymbol{\mu}$ configuration. Thus identifying the $\boldsymbol{\mu}$-independent quantity $I_0(\boldsymbol{\mu})^2 - [\Delta I_P(\boldsymbol{\mu})/P]^2$, a characteristic of the magnetic materials, for two different magnetic configurations $\boldsymbol{\mu}$ and $\boldsymbol{\mu}'$, we obtain the relation

$$1 - \left(\frac{I_0(\boldsymbol{\mu}')}{I_0(\boldsymbol{\mu})}\right)^2 = \left[1 - \left(\frac{\Delta I_P(\boldsymbol{\mu}')}{\Delta I_P(\boldsymbol{\mu})}\right)^2\right] s(\boldsymbol{\mu})^2 \tag{A19}$$

which allows us to determine both $s(\boldsymbol{\mu})$ and P *independently*. This relation involves $\Delta I_P(\boldsymbol{\mu}')/\Delta I_P(\boldsymbol{\mu})$ and $I_0(\boldsymbol{\mu}')/I_0(\boldsymbol{\mu})$ ratios, which are characteristics of the magnetic structure.

In a ferromagnetic bilayer, we replace the $\boldsymbol{\mu}$ vector by F (AF) to refer to the absolute value of quantities respectively measured in any of the two F (AF) configurations. If the magnetic films have comparable spin selectivities, $s(\mathrm{AF}) \ll 1$. Thus in the relation $[1 - s(F)^2] I_0(F)^2 = [1 - s(\mathrm{AF})^2] I_0(\mathrm{AF})^2$ [see Eq. (A18)], $s(\mathrm{AF})^2$ can be neglected to determine $s(F)$ from the ratio of the transmitted currents in the F and AF states, measured with an unpolarized electron beam. In an IMFP model, if both layers of thicknesses d_1 and d_2 are made from the same material, we have $s(\mathrm{AF}) = \tanh|(d_1 - d_2)/\delta|$ and $s(F) = \tanh|(d_1 + d_2)/\delta|$, which allows us to determine δ. In fact, in Ref. 22, this technique was used by injecting a moderate-energy beam (10 eV) through a Au/Co/Au/Co/Au structure. At the entrance plane, a secondary-electron distribution is formed in gold and, subsequently ballistic-electron transmission arises through the sample, most of the emitted current being transported at an energy close to the vacuum level of the exit face, lowered down to about 2 eV by cesium deposition, where the IMFP is larger. Then, relevant information is extracted from the low-energy part of the spectrum. By this way, there is also no doubt that the detected electrons interacted with the metal foil.

[1] J. J. Quinn, Phys. Rev. **126**, 1453 (1962).
[2] M. P. Seah and W. A. Dench, Surf. Interface Anal. **1**, 2 (1979).
[3] H. C. Siegmann, J. Phys.: Condens. Matter **4**, 8395 (1992).
[4] R. W. Rendell and D. R. Penn, Phys. Rev. Lett. **45**, 2057 (1980).
[5] J. Hong and D. L. Mills, Phys. Rev. B **59**, 13 840 (1999).
[6] E. Vescovo, C. Carbone, U. Alkemper, O. Rader, T. Kachel, W. Gudat, and W. Eberhardt, Phys. Rev. B **52**, 13 497 (1995).
[7] C. N. Berglund and W. E. Spicer, Phys. Rev. **136**, A1030 (1964).
[8] C. N. Berglund and W. E. Spicer, Phys. Rev. **136**, A1044 (1964).
[9] W. F. Krolikowski and W. E. Spicer, Phys. Rev. **185**, 882 (1969).
[10] W. F. Krolikowski and W. E. Spicer, Phys. Rev. B **1**, 478 (1970).
[11] D. E. Eastman, Solid State Commun. **8**, 41 (1970).
[12] D. T. Pierce and H. C. Siegmann, Phys. Rev. B **9**, 4035 (1974).
[13] D. Oberli, R. Burgermeister, S. Riesen, W. Weber, and H. C. Siegmann, Phys. Rev. Lett. **81**, 4228 (1998).
[14] G. Schönhense and H. C. Siegmann, Ann. Phys. (Leipzig) **2**, 465 (1993).
[15] C. Kittel, *Introduction to Solid State Physics* (Wiley, New York, 1971).
[16] H. C. Siegmann, Surf. Sci. **307–309**, 1076 (1994).
[17] H.-J. Drouhin, Phys. Rev. B **56**, 14 886 (1997).
[18] E. O. Kane, Phys. Rev. **159**, 624 (1967).
[19] D. R. Penn, S. P. Apell, and S. M. Girvin, Phys. Rev. B **32**, 7753 (1985).
[20] D. A. Papaconstantopulos, *Handbook of the Band Structure of Elemental Solids* (Plenum, New York, 1986).
[21] J. S. Helman and W. Baltensperger, Phys. Rev. B **22**, 1300 (1980).
[22] H.-J. Drouhin, C. Cacho, G. Lampel, Y. Lassailly, J. Peretti, and A. J. van der Sluijs, *Proceedings of Low Energy Polarized Electron Workshop*, edited by Y. A. Mamaev, S. A. Starovoitov, T. V. Vorobyeva, and A. N. Ambrazhei (PES Lab Publishing, St. Petersburg, 1998), p. 79; H.-J. Drouhin, C. Cacho, G. Lampel, Y. Lassailly, and J. Peretti (unpublished).
[23] M. Getzlaff, J. Bansmann, and G. Schönhense, Solid State Commun. **87**, 467 (1993).
[24] D. P. Pappas, K.-P. Kämper, B. P. Miller, H. Hopster, D. E. Fowler, C. R. Brundle, A. C. Luntz, and Z.-X. Shen, Phys. Rev. Lett. **66**, 504 (1991).
[25] A. Filipe, H.-J. Drouhin, G. Lampel, Y. Lassailly, J. Nagle, J.

Peretti, V. I. Safarov, and A. Schuhl, Phys. Rev. Lett. **80**, 2425 (1998).
[26] J.-P. Renard, P. Bruno, R. Mégy, B. Bartenlian, P. Beauvillain, C. Chappert, C. Dupas, E. Kolb, M. Mulloy, P. Veillet, and E. Vélu, Phys. Rev. B **51**, 12 821 (1995).
[27] O. Paul, Ph.D. Dissertation, ETH Zürich, 1990.
[28] J. C. Ashley and R. H. Ritchie, Phys. Status Solidi B **83**, K159 (1977).
[29] C. J. Tung, J. C. Ashley, and R. H. Ritchie, Surf. Sci. **81**, 427 (1979).
[30] H. Kanter, Phys. Rev. B **1**, 522 (1970).
[31] I. Lindau, P. Pianetta, R. K. Yu, and W. E. Spicer, J. Electron Spectrosc. Relat. Phenom. **8**, 487 (1976).
[32] D. Norman and D. P. Woodruff, Solid State Commun. **22**, 711 (1977).
[33] H.-J. Drouhin, A. J. van der Sluijs, Y. Lassailly, and G. Lampel, J. Appl. Phys. **79**, 4734 (1996).